ADVANCED FUNCTIONAL MATERIALS
www.afm-journal.de

Meeting High Stability and Efficiency in Hybrid Light-Emitting Diodes Based on SiO_2/ZrO_2 Coated $CsPbBr_3$ Perovskite Nanocrystals

Yanyan Duan, Cintia Ezquerro, Elena Serrano, Elena Lalinde, Javier García-Martínez, Jesús R. Berenguer,* and Rubén D. Costa**

Significant advances are realized in perovskite-converted hybrid light-emitting diodes (pc-HLEDs). However, long-living devices at high efficiencies still represent a major milestone with average stabilities of <200 h at ≈50 lm W^{-1} under low applied currents (<15 mA). Herein, a dual metal oxide-coated $CsPbBr_3@SiO_2/ZrO_2$ composite is prepared in a one-pot synthesis through the kinetic control of the sol–gel reaction, followed by a gentle drying process in air. These hybrid nanoparticles show photoluminescence quantum yields of ≈65% that are stable under temperature, ambient, and irradiation stress scenarios. This is translated to pc-HLEDs with a near-unity conversion efficiency at any applied current, high efficiencies around 75 lm W^{-1}, and one of the most remarkable stabilities of ≈200 and 700 h at 100 and 10 mA, respectively. In addition, the device degradation mechanism is thoughtfully rationalized comparing devices operating under ambient/inert conditions. As such, this work provides three milestones: i) a new room temperature one-pot protocol to realize the first SiO_2/ZrO_2 metal oxide coating that effectively protects the emitting perovskite nanoparticle core, ii) one of the most stable and efficient pc-HLEDs operating under ambient condition at any applied current, and iii) new insights for the degradation of pc-HLEDs.

1. Introduction

Over the past decades, semiconductor nanocrystals or quantum dots (QDs), such as CdS, CdSe, ZnS, and $CuInS_2$, have represented a great promise in lighting and display applications due to their high photoluminescence quantum yields (PLQYs), narrow emission bands, and easy preparation.[1] However, limitations, such as i) the high costs of the synthesis, requiring long time and high temperatures and ii) the low sustainability due to the use of toxic and/or rare earth elements, are considered huge roadblocks towards their wide use as active components in commercial lighting systems.[2] Therefore, the scientific community is highly active in the search of new alternatives for color downconversion purposes.[3]

In this context, huge efforts are being devoted to the development of metal halide perovskites (MHPs) that feature comparable photoluminescence properties to QDs.[4] In short, several groups have stated that the major assets of MHPs are: i) easy color tunability through compositional modulations, as the emission spectra can be tuned from 400 to 700 nm;[2a,5] ii) excellent optical and electronic properties, like high PLQYs (>80%);[6] iii) narrow full width at half maximum (FWHM), enabling them high color purity;[7] iv) wide color gamut, covering up to 120% of the National Television System Committee color standard, which is superior to the commercial OLEDs and QLEDs;[8] v) high defect tolerance;[9] and vi) gentle preparation environment (less than 200 °C).[10]

Y. Y. Duan, Prof. R. D. Costa
IMDEA Materials Institute
Calle Eric Kandel 2, Getafe 28906, Spain
Y. Y. Duan
Departamento de Ciencia de Materiales
Universidad Politécnica de Madrid
E.T.S. de Ingenieros de Caminos
Profesor Aranguren s/n
Madrid 28040, Spain

The ORCID identification number(s) for the author(s) of this article can be found under https://doi.org/10.1002/adfm.202005401.

DOI: 10.1002/adfm.202005401

Dr. C. Ezquerro, Prof. E. Lalinde, Dr. J. R. Berenguer
Departamento de Química - Centro de Investigación en Síntesis Química (CISQ)
Universidad de La Rioja
Logroño 26006, Spain
E-mail: jesus.berenguer@unirioja.es
Dr. E. Serrano, Prof. J. García-Martinez
Laboratorio de Nanotecnología Molecular
Departamento de Química Inorgánica
Carretera Alicante-S. Vicente s/n, Alicante E-03690, Spain
E-mail: j.garcia@ua.es
Prof. R. D. Costa
Chair of Biogenic Functional Materials
Technical University of Munich
Schulgasse 22, Straubing D-94315, Germany
E-mail: ruben.costa@tum.de

All these merits, especially the unique low synthesis cost,[11] highly tunable bandgap,[12] and narrow emission width,[13] fuel a high interest in the adoption of these emissive materials as phosphor-converted hybrid light-emitting diodes (pc-HLEDs).[1d,14] This lighting concept consists in highly efficient blue-emitting chips, made of InGaP. The chips are covered by a color down-converting filter, which is based on inorganic phosphors doped with rare-earth metals, i.e., cerium-doped yttrium aluminium garnet.[1d,15] Owing to its high luminous efficiency and stability, they are widely used for screen backlighting, indoor and front-lights in automotive, signaling, etc.[16] The main drawback of this approach is the use of inorganic phosphors, as it represents 20–40% of the cost of the lighting system, the lack of recycling protocols, and the limited availability of its components. As above stated, CdSe-QDs could be considered as a short-termed alternative[17] and whole merits of MHPs stablish themselves as a more suitable solution.[18] Here, the major challenge is still the improvement of MHPs stability working under ambient conditions—i.e., photoinduced degradation in the presence of oxygen and moisture—without compromising the device efficiency.[19] Therefore, many groups have focused on enhancing the self-stability of MHPs under ambient conditions using surface engineering[20] and compositional modulation.[21] The former represents the most promising strategy, since, for instance, metal oxides shells—e.g., TiO_2, Al_2O_3, SiO_2, ZrO_2—have been widely adopted to protect QDs.[13a,22] Among them, TiO_2 and Al_2O_3 are not totally transparent, which severely affect the device performance of pc-HLEDs.[20b,22e,23] As far as SiO_2 coating is concerned, its excellent stability against environmental stresses and its transparent characteristics make it as the most popular candidate among different coating materials.[13a,18a,22f] Significant advances in pc-HLEDs using MHPs@SiO_2 have been reported, realizing recorded stabilities of <230 h and efficiencies of <62 lm W^{-1} at 20 mA.[24] Despite the enhanced device performance, the SiO_2 coating is not ideal against ambient storage and operational conditions because of its mesoporous nature. In a recent report, Li's group has reported a ceramic-like stable $CsPbBr_3$ nanocrystals with a recorded stability of 1000 h, maintaining the initial intensity at 20 mA without indicating the device efficiency.[18b] In this system, the dense SiO_2 coating was achieved under harsh conditions, using high sintering temperature of ≈900 °C. Thus, this energy intensive synthesis might hamper the wide use of this ceramic-like emitter in pc-HLEDs. The same group has also reported a SiO_2/Al_2O_3 double coating for the MHPs through using an Al–Si single precursor. This led to enhanced device stabilities of up to 100 h (10% loss of initial luminous intensity) at 5 mA.[25] This is in line with the prior art observed for other materials, in which their coatings with multiple metal oxides have provided a more effective protection than that of individual ones.[26] Moreover, most of the previously commented approaches involve multistep procedures, including formation and isolation of the MHPs and subsequent oxide coating.[13a,18a,22a,c–g] These observations set the relevance of accomplishing an easy and reproducible procedure for the achievement of a protective coating for the MHPs while maintaining their original optical properties.

Finally, most of the previous works mainly focused on improving the operational stability and efficiency of the MHPs and the corresponding pc-HLEDs.[13a,18,25] However, limited attention has been paid to the investigation of the device degradation mechanism up to now. Understanding the degradation process can be more meaningful and important than just improving their performances with regards to the application of the MHPs-based pc-HLEDs.

Herein, this work describes the formation of SiO_2/ZrO_2 protective coating for the preparation of hybrid $CsPbBr_3$@SiO_2/ZrO_2 without affecting the excellent photoluminescence features, i.e., narrow emission bands (FWHM < 20 nm) and high PLQYs (≈65%). The main benefits of the use of ZrO_2 are: i) a highly transparent coating in the whole visible range, ii) easy synthesis in a one-pot method, following a sequential sol–gel process and a gentle drying at ambient conditions, and iii) a highly compact and chemically inert layer that effectively protects the MHPs under ambient storage as well as temperature and water stress scenarios. This results in one of the most stable and efficient pc-HLEDs reported up to date, achieving ≈200 h and 75 lm W^{-1} as well as ≈700 h and 70 lm W^{-1} operating under ambient conditions at 100 and 10 mA, respectively. In addition, the degradation mechanism was thoughtfully investigated, and it was found that the changes in the brightness featured a three-step degradation process.

In light of all of the aforementioned developments, this work presents three milestones in the field of hybrid MHPs@double metal oxide for pc-HLEDs, namely i) the first reported one-pot SiO_2/ZrO_2 oxide coating approach for MHPs, which keeps their excellent photoluminescence properties, ii) one of the best performing pc-HLEDs reported up to date, and iii) new insights for the degradation process of pc-HLEDs through comparing devices operating under ambient and inert conditions.

2. Results and Discussion

2.1. Synthesis and Characterization of $CsPbBr_3$@SiO_2/ZrO_2

The hybrid $CsPbBr_3$@SiO_2/ZrO_2 composite was obtained by a sequential one-pot sol gel strategy following a similar methodology that was described by Yu's group[24] (**Scheme 1**, see the Experimental Section). In short, green emitting $CsPbBr_3$ nanocrystals were first prepared by the hot-injection (140 °C) of a preformed cesium oleate solution into a $PbBr_2$ solution, both in octadecene (ODE) (Scheme 1,i). The $PbBr_2$ solution contains oleic acid (OA) and (3-aminopropyl)triethoxysilane (APTES) as capping agents for the control of the growth of the perovskite nanocrystals. The final used Cs:Pb molar ratio was 1:2.53. After fast cooling at room temperature (RT), the reaction medium was opened to the air and stirred at RT for 3 h. Air moisture induces the formation of an initial silica layer around the MHPs by the slow hydrolysis of the terminal alkoxysilane groups of APTES (Scheme 1,ii). After this step, the zirconia source—i.e., zirconium(IV) tert-butoxide (ZTB)—was added dropwise, reaching a $CsPbBr_3$:APTES:ZTB molar ratio of 1:28.5:8.5. Taking advantage of the presence of trace amount of water in the reaction medium, the reaction flask was closed, and the mixture was further stirred for 3 h at RT, achieving the formation of the final SiO_2/ZrO_2 coating protecting the MHPs (Scheme 1,iii). Finally, the reaction mixture was centrifuged and the obtained solids were washed out with hexane, and air dried

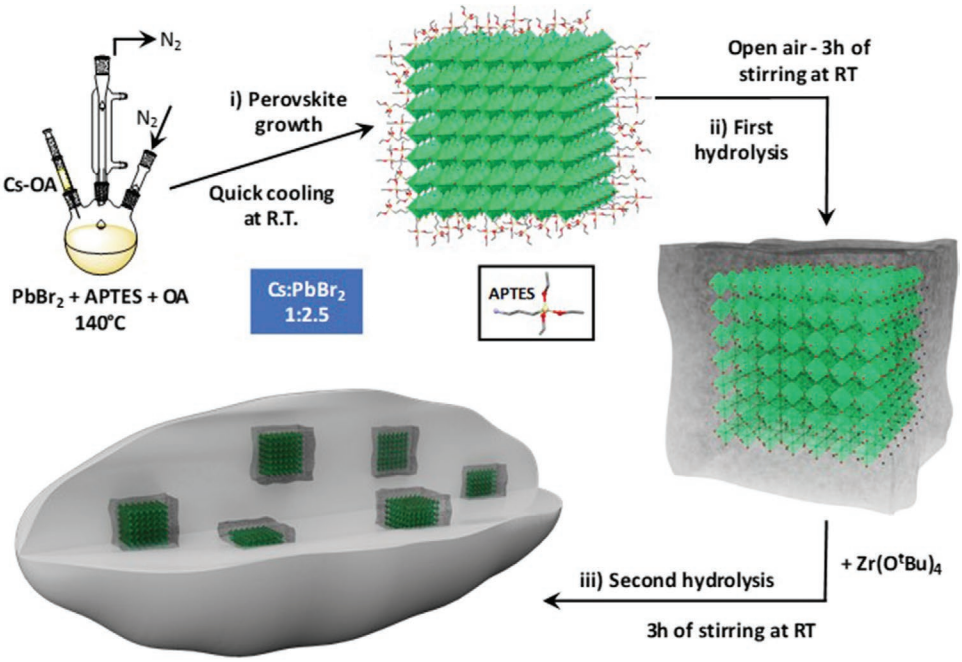

Scheme 1. Schematic representation of the sequential one-pot synthesis of the hybrid $CsPbBr_3@SiO_2/ZrO_2$ composite (Cs-OA refers to the solution of cesium oleate in oleic acid).

overnight. It is worth noting that this straightforward method produces a very stable and highly emissive material, being also easily scalable.

TEM analysis of the perovskite nanoparticles was carried out before and after the formation of the SiO_2/ZrO_2 coating (see **Figure 1**, Figures S1 and S2, Supporting Information, and

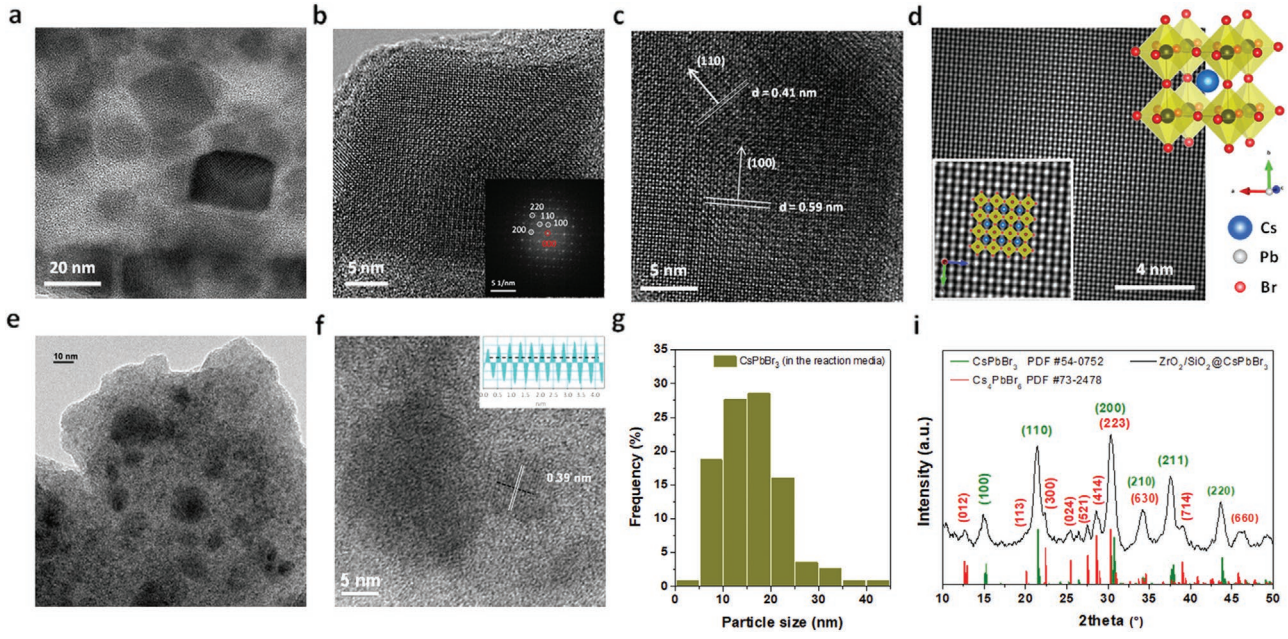

Figure 1. a–d,g) HRTEM analysis of a nonpurified suspension of $CsPbBr_3$. A drop of the suspension taken from the reaction medium before the initial hydrolysis of APTES was added to the grid and air dried overnight (sample $CsPbBr_3@APTES$): a) HRTEM image at low magnification; b) HR-TEM image of a single crystal of $CsPbBr_3$. The inset shows the corresponding FFT; c) region of the HR-TEM image shown in (b) that was used for image analysis, showing lattice fringes with a d-spacing of 0.59 and 0.41 nm, which are consistent with the (100) and (110) planes, respectively, of the cubic phase of $CsPbBr_3$; d) reconstructed image obtained by autocorrelating the image shown in (c) displaying the simulated crystal structure of cubic $CsPbBr_3$ along the normal to (100) plane (upward vector [1–10]); g) histogram showing the particle size distribution of $CsPbBr_3$, estimated from TEM analysis ($n = 120$). e,f,i) Characterization of $CsPbBr_3@SiO_2/ZrO_2$ powders after purification: e,f) TEM images at two different magnifications and i) XRD patterns. For comparison purposes, the PDF cards of the cubic $CsPbBr_3$ (PDF Card No. #54-0752, green lines) and hexagonal Cs_4PbBr_6 (PDF Card No. #73-2478, red lines) references were included in (i).

the Experimental Section). Figure 1a shows $CsPbBr_3$ nanocrystals with a platelet morphology and an average diameter of ≈16 nm (Figure 1g). Note that this is only an approximate value due to the difficulty to measure the crystal sizes from a sample taken directly from the reaction medium. High-resolution TEM (HRTEM) was used to analyze the microstructure of the $CsPbBr_3$ crystals before the silica and zirconia coatings were formed. A typical HRTEM image of a $CsPbBr_3$ single crystal is shown in Figure 1b. This image reveals the cubic structure of $CsPbBr_3$ (100) and (110) lattice fringes with a d-spacing of 0.59 and 0.41 nm, respectively (see Figure 1c). The fast Fourier transform (FFT) of this HRTEM image is shown in the inset of Figure 1b, whose arrayed spots are consistent with a cubic phase. The reconstructed image obtained by autocorrelating the image shown in Figure 1c displays the simulated crystal structure of cubic $CsPbBr_3$ along the normal to (100) plane (upward vector [1–10]) (Figure 1d). The corresponding elemental (Cs, Pb, Br, and Si) mapping obtained by energy-dispersive X-ray spectroscopy (EDX) of this sample shows the uniformity of the elemental distribution in the perovskite crystals (Figure S1, Supporting Information). It should be noted that sample preparation for HRTEM-EDX analysis is done by adding a drop of the suspension taken from the reaction medium, before the initial APTES hydrolysis, to a grid and let it air dry overnight. Thus, APTES hydrolyses during the drying process and this is the reason why silicon appears covering the whole sample in Figure S1 in the Supporting Information. The HRTEM-EDX analysis of the material after the hydrolysis of APTES reveals the presence of silica around the perovskite crystals in the sample $CsPbBr_3@SiO_2$ (Figure S2, Supporting Information).

The morphology of the $CsPbBr_3@SiO_2/ZrO_2$ particles after purification is shown in Figure 1e,f. The perovskites nanoparticles are well dispersed in the SiO_2/ZrO_2 matrix, showing an interplanar spacing of 0.39 nm in Figure 1f, which is consistent with the (110) lattice planes of the cubic structure (d^{XRD}_{110} = 0.41 nm). No clear lattice spacing is found in the light part of TEM images shown in Figure 1e, which might be ascribed to the amorphous nature of the SiO_2 and the relatively poor crystallinity of the ZrO_2 formed at RT. In line with previous SiO_2-protected $CsPbBr_3$ materials,[24] the overall hydrolysis process for the formation of the SiO_2/ZrO_2 matrix prevents the further growth of the perovskite particles. In accordance with this fact, the final SiO_2/ZrO_2 coating does not induce significant changes in the optical properties of the perovskite core, as the emission is closely related to the size of the nanoparticles—vide infra. Furthermore, scanning electronic microscopy (SEM)–energy dispersive spectrometer (EDS) mapping results corroborate the homogeneous distribution of ZrO_2 and SiO_2 (Figure S3 in the Supporting Information). This is in line with the very low adsorption capacity of the $CsPbBr_3@SiO_2/ZrO_2$ composite, which displays a total pore volume of less than 0.01 $cm^3\ g^{-1}$, confirming the dense nature of the SiO_2/ZrO_2 coating. Finally, the XRD patterns of the $CsPbBr_3@SiO_2/ZrO_2$ support the successful formation of cubic $CsPbBr_3$ perovskite. Figure 1i displays diffraction peaks at around 14.9°, 21.4°, 30.5°, 34.2°, 37.6°, and 43.6° that correspond to the crystal planes of (100), (110), (200), (210), (211), and (300), respectively, characteristic of the cubic $CsPbBr_3$ phase[27]—portable document format (PDF) Card No. #54-0752, green lines. In addition, the presence of hexagonal Cs_4PbBr_6 phase is also observed—PDF Card No. #73-2478, red lines. Nevertheless, a direct comparison between the integrated intensities of the main diffraction peaks of both structures suggests that the main crystalline phase is the cubic $CsPbBr_3$, as supported by TEM analysis of the perovskite nanoparticles before reaction (Figures 1a–d). The crystalline domain calculated with the Scherrer equation is ≈10 nm, which confirms the overestimation error associated to TEM inspection, ca. 15 nm (Figure 1g,i).

2.2. Preparation and Characterization of $CsPbBr_3@SiO_2/ZrO_2$/PMMA Color Filters

Self-standing $CsPbBr_3@SiO_2/ZrO_2$ based color filters for pc-HLEDs were prepared through embedding the nanoparticles into a polymethyl methacrylate (PMMA) matrix (see the Experimental Section). This packaging was chosen due to i) its good transparency and processability, ii) excellent thermal stability, and iii) the outstanding compatibility of MHP coatings applied to pc-HLEDs.[15,28] The amount of the hybrid nanoparticles (1 mg) was optimized to ensure a quantitative conversion efficiency in devices—vide infra.

These filters show a highly intense green emission band (λ_{max} = 524 nm and FWHM = 16 nm) associated to PLQYs of ≈65% and $<\tau>$ of 30.6 ns (**Figure 2**c,e and Table S1, Supporting Information). For reference purposes, both the $CsPbBr_3@SiO_2$ solution and the $CsPbBr_3@SiO_2/ZrO_2$ nanoparticles feature a highly intense green emission similar to the bare $CsPbBr_3$ nanoparticles (Figure 2a,b).[18b,24,29] The emission band of the powder is centered at 524 nm with a FWHM of 24 nm that is associated to PLQYs of ≈55% and average excited state lifetime ($<\tau>$) of 30 ns (Figure 2d and Table S1, Supporting Information). As such, the slight enhancement of the photoluminescence behavior in fliter compared to that in powder might be related to the previously described surface passivation of nonradiative defects using PMMA.[1d,22b]

In a next step, we studied the stability of these filters upon storage and temperature stress under ambient conditions. These films show an excellent stability over 30 days under ambient storage conditions, as the PLQY holds constant – **Figure 3**a. The thermal stability was studied via placing these filters onto a heating station, monitoring the emission band changes upon increasing the temperature from RT to 120 °C and then cooled down to RT. In line with the literature,[24] the filters exhibit an exponential temperature-induced emission quenching, reaching a ≈60% intensity loss at 70 °C and an almost quantitative quenching at 120 °C (Figure 3b). The emission band does not show significant changes neither in the λ_{max} nor in the FWHM values during the thermal stress assay (Figure S4a, Supporting Information). This indicates that the thermal quenching is not related to temperature-induced aggregation of the MHPs,[1d] since the average size of the perovskite remains constant. Therefore, the nature of the thermal quenching is mostly due to the temperature induced formation of halogen vacancy traps.[30] Indeed, this process leads to an irreversible loss in the emission intensity, since it is exponentially recovered up to a maximum of ≈70% of the initial value after being exposed to RT and dark

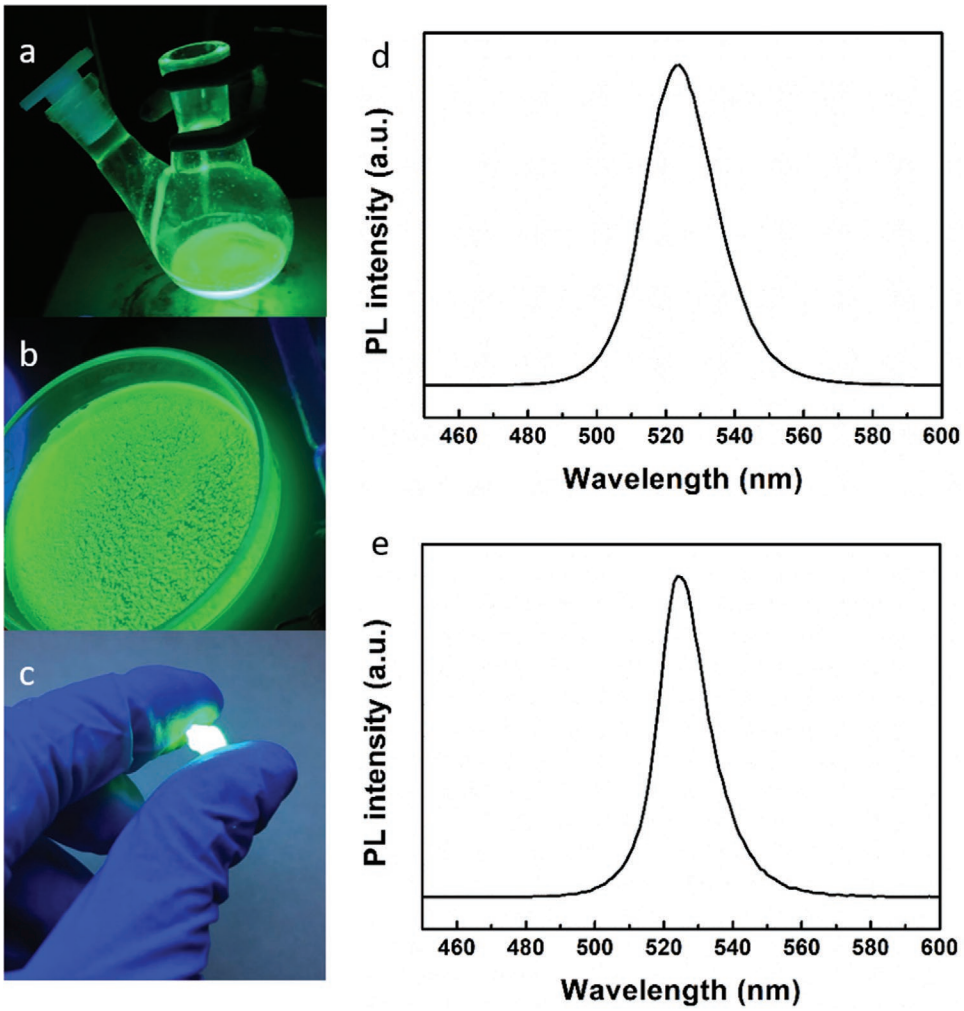

Figure 2. Left: Photographs of a) the reaction medium before the addition of ZTB, b) $CsPbBr_3@SiO_2/ZrO_2$ powder, and c) $CsPbBr_3@SiO_2/ZrO_2$/PMMA filters under UV irradiation (6 W, 370 nm). Right: Emission spectra (λ_{exc} = 370 nm) of d) $CsPbBr_3@SiO_2/ZrO_2$ powders and e) $CsPbBr_3@$ SiO_2/ZrO_2/PMMA filters.

conditions for 24 h (Figure 3b and Figure S4b, Supporting Information). Finally, we also investigated the isothermal stability at 60 °C under dark and ambient conditions, noting neglectable emission changes after 24 h (Figure 3c). The relevance of these findings is highlighted by the direct comparison with the thermal stability noted for the $CsPbBr_3@SiO_2$,[24] in which the emission is totally vanished after increasing the temperature up to 70 °C, without describing any recovery upon cooling to RT. Thus, the second ZrO_2 layer represents an effective strategy to compensate the coating provided by the SiO_2 layer, further protecting the perovskite core from the surrounding environment. To further corroborate this statement, we monitored the changes of the PLQYs by immersing the samples in an aqueous solution. The PLQY slowly decreases, reaching a value of around 30% after one week (Figure 3d). After that, it does not show any obvious change until the 17th day, while it further reduces to 15% after 1 month from the beginning of the experiment. In this case, no recovery was noted after drying. These values are among those reported in the literatures for SiO_2-coated perovskite nanoparticles.[13a,24,29]

2.3. Preparation and Characterization of $CsPbBr_3@SiO_2/ZrO_2$/PMMA Based pc-HLEDs

The devices were prepared by covering the blue-emitting chip of a commercial LED (3 W, 440 nm) using films of PMMA with and without $CsPbBr_3@SiO_2/ZrO_2$ in a remote configuration (see the Experimental Section). As a reference, devices with only PMMA filters show the same narrow emission of the commercial LED, reaching a similar maximal luminous efficiency of ≈15 lm W^{-1} at applied current of 20 mA (**Figure 4**a,b). The efficiency gradually decreases at high applied currents due to the internal loss of the exciton formation at the emitting chips. Devices with $CsPbBr_3@SiO_2/ZrO_2$/PMMA filters show a quantitative blue-to-green conversion regardless of the applied current range (5–200 mA) (Figure 4c). The pc-HLED features a narrow green emission centered at 524 nm that nicely corresponds to that of the hybrid $CsPbBr_3@SiO_2/ZrO_2$ nanoparticles. The luminous efficiency reaches maximal values of 70–75 lm W^{-1} in the 10–100 mA range and slowly decreases to 50 lm W^{-1} at 200 mA (Figure 4d).

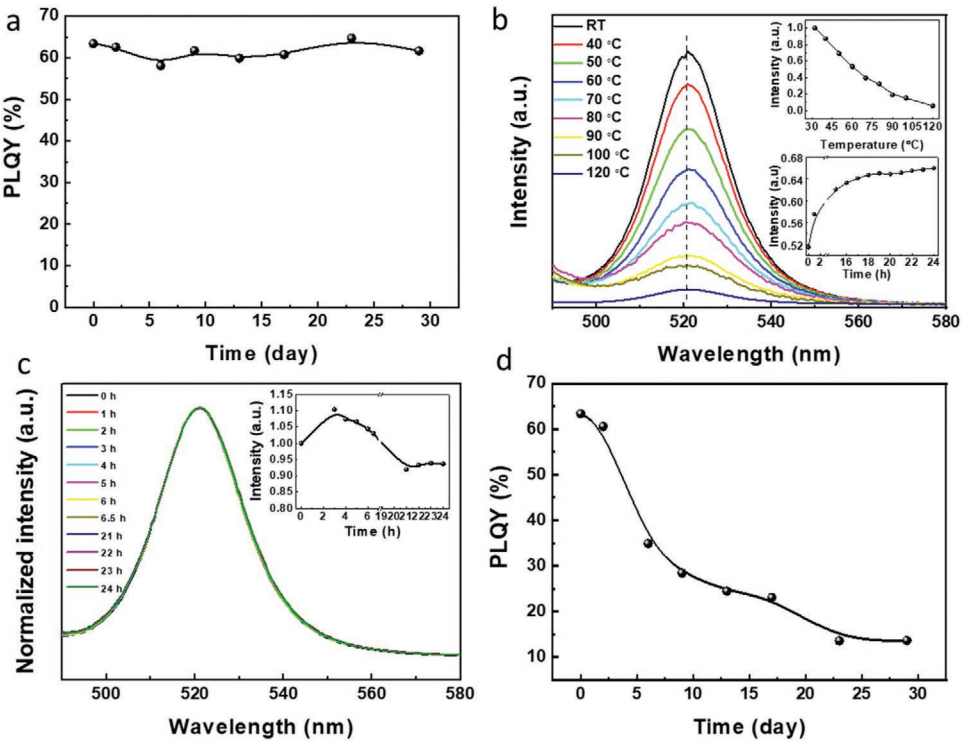

Figure 3. Stability measurement of the $CsPbBr_3$@SiO_2/ZrO_2/PMMA filters. a) Changes of the PLQYs over time under ambient storage conditions. b) Temperature dependent emission spectra and the intensity loss upon heating (top inset) and the intensity recovery over time at RT (bottom inset). c) Changes of the emission spectra and its intensity (inset) at 60 °C for 24 h. d) Changes of the PLQYs after being immersed in aqueous solution over time.

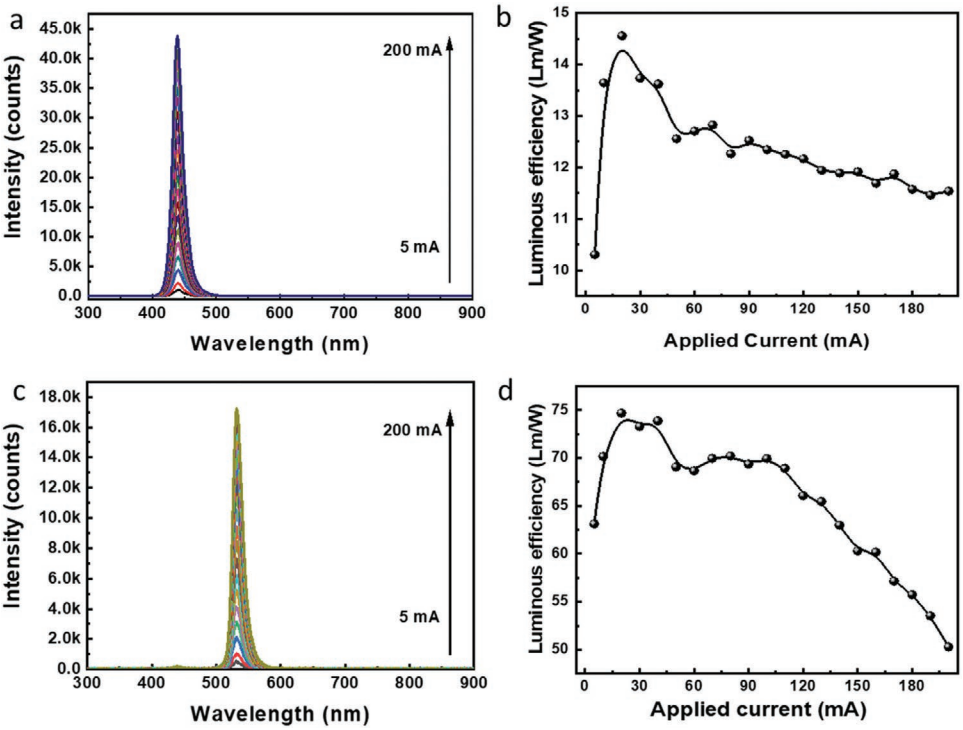

Figure 4. Changes of the emission spectra (left) and luminous efficiency (right) of devices with a,b) PMMA and c,d) $CsPbBr_3$@SiO_2/ZrO_2/PMMA filters placed on the 440 nm LED chip operating at different applied currents.

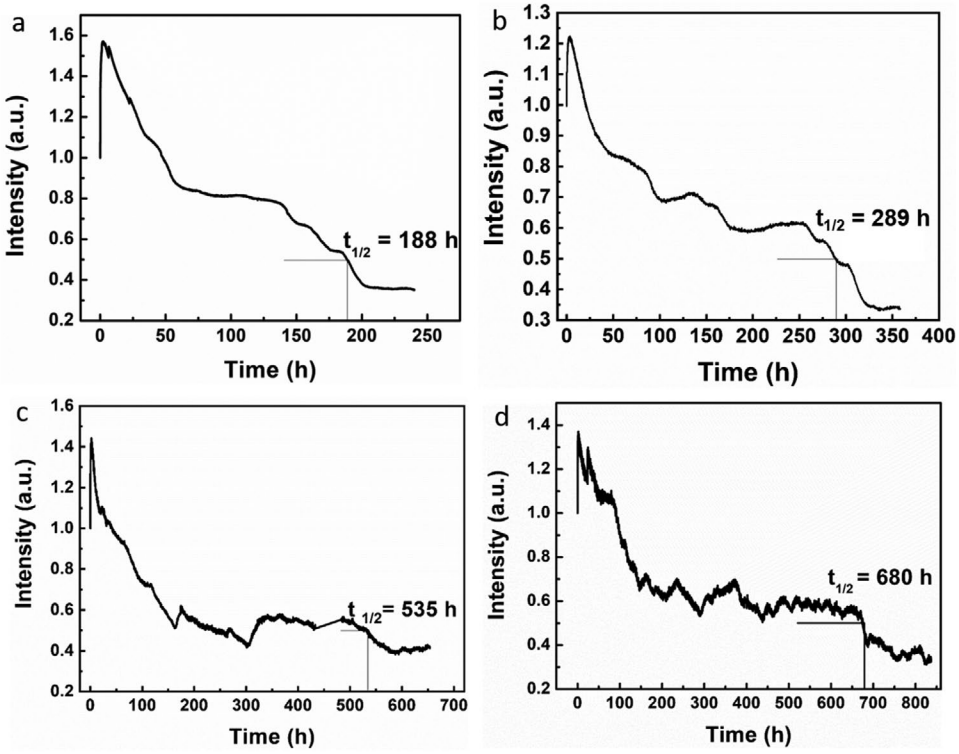

Figure 5. Changes in the device brightness using $CsPbBr_3$@SiO_2/ZrO_2/PMMA filters operating under ambient conditions at applied currents of a) 100, b) 50, c) 15, and d) 10 mA, respectively.

Next, the device stability was assessed by recording the time required to reach 50% of the initial brightness ($t_{1/2}$) at 100, 50, 15, and 10 mA. Regardless of the applied currents, the emission intensity decreases without affecting the shape of the emission band (**Figure 5** and Figures S5–S8, Supporting Information). Importantly, the deactivation process is mainly caused by the constant blue irradiation, since the temperature of the filters held close to 32 °C for all the above operational conditions. Interestingly, the changes in the brightness feature a three-step process (Figure 5 and Table S2, Supporting Information). First, all the devices exhibit an increase in the emission during the first hours (<5 h). This is related to the well-known photoactivation effect, curing the surface traps through removing the dangling bonds.[31] After this quick process, an exponentially decrease of the emission intensity occurs until reaching a plateau at around 60–70% of the initial value that holds for several weeks. Both, the time to reach this plateau and how long it holds, go hand-in-hand with the applied current (Table S2, Supporting Information). This is followed by a final linear decay to 30–40% of the initial value, leading to $t_{1/2}$ of 188, 289, 535, and 680 h at applied currents of 100, 50, 15, and 10 mA, respectively. In contrast to the negligible changes in the shape of the emission band (Figures S5–S8, Supporting Information), both PLQY and $<\tau>$ values of these filters measured after reaching $t_{1/2}$ significantly decreased up to 20–30% and 18–20 ns, respectively. This deactivation is irreversible, since the PLQY values do not recover over time upon storing the filter under dark and ambient conditions. In addition, the excited state lifetime decay obeys a biexponential fitting (Figures S5-S8 and Table S3, Supporting Information), in which the short and long components are related to nonradiative trapping and radiative recombination processes, respectively.[32] Compared to the spectroscopy features of fresh filters, the τ_1 values strongly reduced, indicating a more efficient exciton trapping.

To get further insights into the deactivation process, freshly prepared devices were measured in an inert atmosphere (<0.001 ppm for both water and oxygen) at 100 and 10 mA. In stark contrast to devices operating under ambient conditions, they are less stable, showing a quick exponential deactivation behavior (**Figure 6** and Figure S9, Supporting Information). In both scenarios, we exclude i) the photodegradation of the ligands from the oxide coating due to their high energy band, i.e., SiO_2 (≈8.6 eV) and ZrO_2 (≈5.0 eV) and ii) the photoinduced aggregation as the FWHM and the maximal emission peak hold constant regardless of the operating conditions (Figure S9, Supporting Information). Therefore, the initial emission deactivation might be caused by the formation of surface trapping defects promoted by the photoinduced desorption of the surface ligands, as previously noted for chalcogenide QDs film[33] and $CsPbBr_3$ QD/AlO_x nanocomposites.[22e] The plateau noted for devices measured under ambient conditions might be related to the combination of oxygen, moisture, and blue excitation. We can discard an oxygen-driven process, as the device emission band holds constant over time, while the simultaneous effect of oxygen and blue excitation usually leads to a color change of the emission towards to the yellow region.[31a] Thus, the differences in device stability might be attributed to the presence of moisture that promotes the plateau stage.

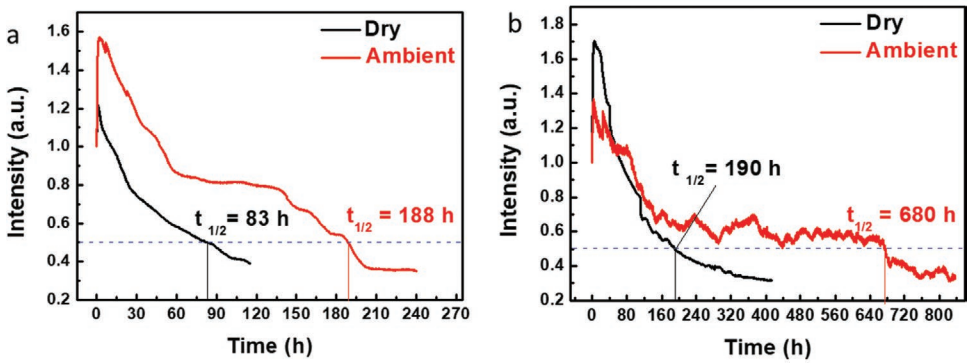

Figure 6. Changes in the device brightness using $CsPbBr_3$@SiO_2/ZrO_2/PMMA filters operating under ambient/dry conditions at a) 100 mA and b) 10 mA.

This is in line with previous reports, in which a gentle surface hydration process can passivate surface trap-states, increasing the photostability of similar MHPs.[13a] In addition, this moisture-induced enhancement behavior has also been reported in other works for lead-free $Cs_3Bi_2Br_9$ NCs,[34] $MAPbI_3$ film,[35] as well as the bare $CsPbBr_3$ solution.[36] However, severe surface degradation will occur after being continuously exposed to the moisture and constant blue excitation, and this will cause an emission deactivation.[37] At this stage, the emission color is still not being affected (see Figures S5–S8, Supporting Information). Thus, the SiO_2/ZrO_2 coating provides an effective barrier against a quick hydration of the surface of the nanoparticles, which is key to realize highly stable pc-HLEDs. Further experiments are on-going in our laboratories for the in situ monitoring of surface changes of the MHPs under device operating conditions.

In order to contextualize the relevance of our results, **Table 1** provides a direct comparison concerning to the PLQYs, the device structure, and the device figures of merit (efficiency and stability) of $CsPbBr_3$ nanoparticles used in pc-HLEDs. These data highlight the relevance of our pc-HLEDs based on $CsPbBr_3$@SiO_2/ZrO_2/PMMA filters that can be considered as one of the most efficient and stable devices reported up to date.

3. Conclusions

A RT one-pot process for the SiO_2/ZrO_2 coating of highly emissive $CsPbBr_3$ perovskites is reported and their performsnces have been systematically tested. This simple and easily scalable method significantly enhances the storage, thermal, moisture, and irradiation stabilities of the perovskite nanocrystals, without affecting their photoluminescence properties. Using this strategy, we produced highly performing $CsPbBr_3$@SiO_2/ZrO_2/PMMA color filters used to quantitatively downconvert the blue emission of LEDs at any applied current ranging from 5 to 200 mA. In addition, these pc-HLEDs combine high efficiencies of 70–75 lm W^{-1} and stabilities of ≈200 and 700 h operating under ambient conditions at 100 and 10 mA, respectively. Their deactivation process is related to an initial quick photoinduced desorption of the surface ligands that promotes the formation of surface trapping defects. However, the SiO_2/ZrO_2 coating hinders the surface hydration process that initially passivates the surface trap-states, leading to a long-living plateau stage and, in turn, yielding to highly stable pc-HLEDs. Unfortunately, the long exposition to moisture under continuous blue excitation is still detrimental for the device stability, even when a dense coating is used. Overall, the adoption of the SiO_2/ZrO_2 coating opens up an alternative approach for the encapsulation of the MHPs

Table 1. Comparison of the PLQYs of hybrid $CsPbBr_3$@metal oxide nanoparticles, the device structure, luminous efficacy, and stability of their respective pc-LEDs.

Composites	PLQY [%]	Device structure	Luminous efficiency [Lm W^{-1}]	Device lifetime [% kept/h]	Reference
$CsPbBr_3$-TDPA	68	Blue LED chip/$CsPbBr_3$-TDPA/KSF	63	90/15	[38]
$CsPbBr_3$@ZrO_2	90	Blue LED chip/$CsPbBr_3$@ZrO_2	–	90/3	[22d]
		Blue LED chip/$CsPbBr_3$@ZrO_2/CdSe	55	90/2	
$CsPbBr_3$@SiO_2	71	Blue LED chip/$CsPbBr_3$@SiO_2	–	100/1000	[18b]
$CsPbBr_3$@SiO_2	82	Blue LED chip/$CsPbBr_3$@SiO_2/$CsPb(Br/I)_3$@SiO_2	35.3	100/40	[29]
$CsPbBr_3$@SiO_2	80	Blue LED chip/$CsPbBr_3$@SiO_2/CdSe	56	100/1	[13a]
$CsPbBr_3$@polymer fibers	48	Violet LED chip/$CsPbBr_3$@polymer fibers/CdSe	–	–	[39]
$CsPbBr_3$@CaF_2	82	Blue LED chip/KSF/$CsPbBr_3$@CaF_2	62.7	90/8	[40]
$CsPbBr_3$@SiO_2/Al_2O_3	90	Blue LED chip/$CsPbBr_3$@SiO_2/Al_2O_3	80.8	90/96	[25]
$CsPbBr_3$@SiO_2	85	Blue LED chip/$CsPbBr_3$@SiO_2/$CsPb(Br/I)_3$@SiO_2	61.2	50/227	[24]
$CsPbBr_3$@glass	42	Blue LED chip/$CsPbBr_3$@glass/$CaAlSiN_3:Eu^{2+}$ (CASNE)	50.5	100/15	[41]
$CsPbBr_3$@ SiO_2/ZrO_2	63.39	Blue LED chip/$CsPbBr_3$@SiO_2/ZrO_2	74.7	50/680	This work

to meet highly stable and efficient pc-HLEDs in the near future. Still, the fine control and understanding of MHP stabilization by the use of multiple and dense metal oxides coatings is highly desirable, being part of the on-going work in our laboratories.

4. Experimental Section

General Considerations: Cs_2CO_3 (99.9%), $PbBr_2$ (99.9%), oleic acid (90%), 1-octadecene (90%, ODE), (3-aminopropyl)triethoxysilane (99%, APTES), zirconium(IV) tert-butoxide (99.99%, ZTB), and PMMA (M_W = 350.000) were purchased from Sigma-Aldrich and used as received without further purification. All analytical grade solvents were purified by distillation.

Synthesis of Cesium Oleate: 0.80 g (2.45 mmol) of Cs_2CO_3, 2.50 mL (7.92 mmol) of OA, and 30 mL (0.08 mol) of ODE were degassed and dried under vacuum, first at RT for 10 min and then heated to 120 °C for 1 h. The mixture was further heated at 150 °C under nitrogen for 2 h until a clear solution was obtained.

Synthesis of $CsPbBr_3@SiO_2/ZrO_2$: The initial hot-injection method for the synthesis of the SiO_2/ZrO_2 protected $CsPbBr_3$ follows a modified procedure based on previously published work.[24] Specifically, 10 mL (28.16 mmol) of ODE and 0.138 g (0.38 mmol) of $PbBr_2$ were degassed and dried under vacuum, first for 10 min at RT and then at 120 °C for 1 h. The system was put under N_2 and a mixture of 50 µL (0.16 mmol) of OA and 1 mL (4.27 mmol) of APTES were slowly added to the mixture. After obtaining a clear solution, the temperature was raised to 140 °C and 1 mL of the above cesium oleate solution (preheated to 100 °C) was quickly injected. After 5 s, the reaction was quenched by placing the flask on an ice-water bath. Then, the flask was opened to the air and stirred for 3 h at RT, letting the alkoxysilane terminal groups of APTES start the hydrolysis and condensation processes.

After that, 0.5 mL (1.28 mmol) of ZrO_2 precursor, ZTB, was slowly added to the solution under stirring. The flask was closed with a cup and the mixture reacted for other 3 h at RT, using the residual water (from the air) to achieve the final hydrolysis process. The final suspension was centrifuged at 8000 rpm for 20 min and washed twice with 10 mL of hexane. The obtained yellowish solid was deposited in a petri dish and dried in a fume hood overnight under ambient conditions and the presence of air.

Characterization Techniques: The morphology of the materials was investigated by transmission electron microscopy (TEM) and scanning electron microscopy (SEM). Aliquots of the $CsPbBr_3$ perovskite solution were taken from the reaction medium before adding ZTB, and deposited in a copper grid for TEM observations. $CsPbBr_3@SiO_2/ZrO_2$ powders were suspended in hexane and sonicated for 15 min. A few drops of this suspension were placed on a Lacey Formvar/Carbon copper grid, and the hexane evaporated at RT. High-resolution TEM (HRTEM) and EDX analyses were performed using a JEOL JEM-1400 Plus microscope, while TEM observations were carried out using a JEOL JEM-2010 microscope, at an accelerating voltage of 200 kV. The digital analysis of the TEM images was performed using Digital image TM 3.6.1 by Gatan. Simulated crystal structure of cubic $CsPbBr_3$ was carried out using VESTA software (version 3.4.8, Copyright 2006–2020 y Koichi Momma and Fuji Izumi). SEM-EDS were carried out through the FEI 600i, OXFORD INSTRUMENTS. X-ray powder diffraction (XRD) was performed in a SEIFERT 2002 apparatus using a CuK_α (1.5418 Å) radiation and a scanning velocity of 1° min^{-1}. The photophysical studies were carried out using a FS5 Spectrofluorometer (Edinburgh Instruments) with the SC-10 module for solid samples, the SC-30 Integrating Sphere to determine PLQY, and the 375 nm time-correlated single photo counting (TCSPC) (64.3 ps pulse width) module to determine τ.

Fabrication and Characterization of pc-HLEDs: 1 mg of $CsPbBr_3@SiO_2/ZrO_2$ nanoparticles were dispersed in the PMMA/toluene solution (1/6 g mL^{-1}) under vigorous stirring getting a homogeneous solution. The solution was partially dried under vacuum to increase its viscosity. They were placed in a handmade mold and the solvent was further removed under vacuum. As such, $CsPbBr_3@SiO_2/ZrO_2$/PMMA filters with a thickness of ≈350 µm were obtained. These coatings were placed on top of a LED chip of 440 nm (3W, Winger Electronics) and irradiated at 1–100 mA at ambient (moisture 30% and 25 °C) and inert (N_2 atmosphere, less than 0.001 ppm of moisture and O_2) conditions. The pc-HLEDs were characterized using a Keithley 2400 as a current source, while the changes in the electroluminescence spectrum were monitored using an AVS-DESKTOP-USB2 (Avantes) in conjunction with a calibrated integrated sphere Avasphere 30-Irrad. The efficiency, changes in the color, and the emission intensity were monitored over time. Changes in the coating temperature were preciously monitored using a thermographic camera T430sc (FLIR systems, Inc).

Supporting Information

Supporting Information is available from the Wiley Online Library or from the author.

Acknowledgements

Y.D. and C.E. contributed equally to this work. R.D.C. acknowledges the program "Ayudas para la atracción de talento investigador—Modalidad 1 of the Consejería de Educación, Juventud y Deporte—Comunidad de Madrid with the Reference No. 2016-T1/IND- 1463," Spanish Ministry of Economy and Competitiveness (MINECO) for the Ramón y Cajal program (RYC-2016-20891), and HYNANOSC (RTI2018-099504-A-C22). Y.Y.D. also thanks the financial support from China Scholarship Council (No. 201808440326). This work was supported by the Spanish MICINN and Agencia Estatal de Investigación (AEI)/European Regional Development Fund (FEDER) (Projects CTQ2015-74494-JIN, CTQ2016-78463-P, RTI2018-099504-B-C21/A-C22, and PID2019-109742GB-I00). E.S. thanks Universidad de Alicante through the "Programa de Retención de Talento" (ref. UATALENTO16-03) and C.E. thanks Universidad de La Rioja for a grant. Open access funding enabled and organized by Projekt DEAL.

Conflict of Interest

The authors declare no conflict of interest.

Keywords

color downconverting coatings, hybrid light-emitting diodes, metal oxide, perovskite nanoparticles, silica/zirconia

Received: June 26, 2020
Published online: August 2, 2020

[1] a) J. Zhao, J. A. Bardecker, A. M. Munro, M. S. Liu, Y. Niu, I.-K. Ding, J. Luo, B. Chen, A. K.-Y. Jen, D. S. Ginger, *Nano Lett.* **2006**, *6*, 463; b) Q. Sun, Y. A. Wang, L. S. Li, D. Wang, T. Zhu, J. Xu, C. Yang, Y. Li, *Nat. Photonics* **2007**, *1*, 717; c) C. Czekelius, M. Hilgendorff, L. Spanhel, I. Bedja, M. Lerch, G. Müller, U. Bloeck, D. S. Su, M. Giersig, *Adv. Mater.* **1999**, *11*, 643; d) Y. Wei, Z. Cheng, J. Lin, *Chem. Soc. Rev.* **2019**, *48*, 310.

[2] a) X. Li, Y. Wu, S. Zhang, B. Cai, Y. Gu, J. Song, H. Zeng, *Adv. Funct. Mater.* **2016**, *26*, 2435; b) J. Jasieniak, P. Mulvaney, *J. Am. Chem. Soc.* **2007**, *129*, 2841; c) P.-H. Chuang, C. C. Lin, R.-S. Liu, *ACS Appl. Mater. Interfaces* **2014**, *6*, 15379.

[3] a) L. N. Quan, F. P. Garcia de Arquer, R. P. Sabatini, E. H. Sargent, *Adv. Mater.* **2018**, *30*, 1801996; b) Y. Fu, H. Zhu, J. Chen, M. P. Hautzinger, X. Y. Zhu, S. Jin, *Nat. Rev. Mater.* **2019**, *4*, 169.

[4] a) T. Xuan, J. Huang, H. Liu, S. Lou, L. Cao, W. Gan, R.-S. Liu, J. Wang, *Chem. Mater.* **2019**, *31*, 1042; b) H. Wu, S. Wang, F. Cao, J. Zhou, Q. Wu, H. Wang, X. Li, L. Yin, X. Yang, *Chem. Mater.* **2019**, *31*, 1936; c) C. Peng, X. Song, J. Yin, G. Zhang, H. Fei, *Angew. Chem., Int. Ed.* **2019**, *58*, 7818.

[5] L. Protesescu, S. Yakunin, M. I. Bodnarchuk, F. Krieg, R. Caputo, C. H. Hendon, R. X. Yang, A. Walsh, M. V. Kovalenko, *Nano Lett.* **2015**, *15*, 3692.

[6] a) F. Yan, J. Xing, G. Xing, L. Quan, S. T. Tan, J. Zhao, R. Su, L. Zhang, S. Chen, Y. Zhao, *Nano Lett.* **2018**, *18*, 3157; b) J. Xing, Y. Zhao, M. Askerka, L. N. Quan, X. Gong, W. Zhao, J. Zhao, H. Tan, G. Long, L. Gao, *Nat. Commun.* **2018**, *9*, 3541.

[7] a) H. Cho, C. Wolf, J. S. Kim, H. J. Yun, J. S. Bae, H. Kim, J. M. Heo, S. Ahn, T. W. Lee, *Adv. Mater.* **2017**, *29*, 1700579; b) J. Pan, Y. Shang, J. Yin, M. De Bastiani, W. Peng, I. Dursun, L. Sinatra, A. M. El-Zohry, M. N. Hedhili, A.-H. Emwas, *J. Am. Chem. Soc.* **2017**, *140*, 562.

[8] a) S. Reineke, F. Lindner, G. Schwartz, N. Seidler, K. Walzer, B. Lüssem, K. Leo, *Nature* **2009**, *459*, 234; b) M. Chen, Y. Zou, L. Wu, Q. Pan, D. Yang, H. Hu, Y. Tan, Q. Zhong, Y. Xu, H. Liu, B. Sun, Q. Zhang, *Adv. Funct. Mater.* **2017**, *27*, 1701121; c) Q. Zhou, Z. Bai, W. G. Lu, Y. Wang, B. Zou, H. Zhong, *Adv. Mater.* **2016**, *28*, 9163.

[9] Q. A. Akkerman, G. Raino, M. V. Kovalenko, L. Manna, *Nat. Mater.* **2018**, *17*, 394.

[10] a) G. Xing, N. Mathews, S. S. Lim, N. Yantara, X. Liu, D. Sabba, M. Gratzel, S. Mhaisalkar, T. C. Sum, *Nat. Mater.* **2014**, *13*, 476; b) Z. K. Tan, R. S. Moghaddam, M. L. Lai, P. Docampo, R. Higler, F. Deschler, M. Price, A. Sadhanala, L. M. Pazos, D. Credgington, F. Hanusch, T. Bein, H. J. Snaith, R. H. Friend, *Nat. Nanotechnol.* **2014**, *9*, 687.

[11] D. Han, M. Imran, M. Zhang, S. Chang, X. G. Wu, X. Zhang, J. Tang, M. Wang, S. Ali, X. Li, G. Yu, J. Han, L. Wang, B. Zou, H. Zhong, *ACS Nano* **2018**, *12*, 8808.

[12] Y. Tong, B. J. Bohn, E. Bladt, K. Wang, P. Muller-Buschbaum, S. Bals, A. S. Urban, L. Polavarapu, J. Feldmann, *Angew. Chem., Int. Ed.* **2017**, *56*, 13887.

[13] a) H. Hu, L. Wu, Y. Tan, Q. Zhong, M. Chen, Y. Qiu, D. Yang, B. Sun, Q. Zhang, Y. Yin, *J. Am. Chem. Soc.* **2018**, *140*, 406; b) F. Yan, J. Xing, G. Xing, L. Quan, S. T. Tan, J. Zhao, R. Su, L. Zhang, S. Chen, Y. Zhao, A. Huan, E. H. Sargent, Q. Xiong, H. V. Demir, *Nano Lett.* **2018**, *18*, 3157.

[14] a) F. L. Zeng, M. Yang, J. L. Qin, F. Teng, Y. Q. Wang, G. X. Chen, D. W. Wang, H. S. Peng, *ACS Appl. Mater. Interfaces* **2018**, *10*, 42837; b) X. Tang, W. Chen, Z. Liu, J. Du, Z. Yao, Y. Huang, C. Chen, Z. Yang, T. Shi, W. Hu, Z. Zang, Y. Chen, Y. Leng, *Small* **2019**, *15*, e1900484.

[15] M. Bidikoudi, E. Fresta, R. Costa, *Chem. Commun.* **2018**, *54*, 8150.

[16] a) M. Leng, Y. Yang, K. Zeng, Z. Chen, Z. Tan, S. Li, J. Li, B. Xu, D. Li, M. P. Hautzinger, *Adv. Funct. Mater.* **2018**, *28*, 1704446; b) F. Steranka, J. Bhat, D. Collins, L. Cook, M. Craford, R. Fletcher, N. Gardner, P. Grillot, W. Goetz, M. Keuper, *Phys. Status Solidi A* **2002**, *194*, 380.

[17] H. S. Jang, H. Yang, S. W. Kim, J. Y. Han, S. G. Lee, D. Y. Jeon, *Adv. Mater.* **2008**, *20*, 2696.

[18] a) H. C. Wang, S. Y. Lin, A. C. Tang, B. P. Singh, H. C. Tong, C. Y. Chen, Y. C. Lee, T. L. Tsai, R. S. Liu, *Angew. Chem., Int. Ed.* **2016**, *55*, 7924; b) Q. Zhang, B. Wang, W. Zheng, L. Kong, Q. Wan, C. Zhang, Z. Li, X. Cao, M. Liu, L. Li, *Nat. Commun.* **2020**, *11*, 31.

[19] H. Cho, Y. H. Kim, C. Wolf, H. D. Lee, T. W. Lee, *Adv. Mater.* **2018**, *30*, e1704587.

[20] a) J. Pan, Y. Shang, J. Yin, M. De Bastiani, W. Peng, I. Dursun, L. Sinatra, A. M. El-Zohry, M. N. Hedhili, A. H. Emwas, O. F. Mohammed, Z. Ning, O. M. Bakr, *J. Am. Chem. Soc.* **2018**, *140*, 562; b) Z.-J. Li, E. Hofman, J. Li, A. H. Davis, C.-H. Tung, L.-Z. Wu, W. Zheng, *Adv. Funct. Mater.* **2018**, *28*, 1704288.

[21] a) H. Liu, Z. Wu, J. Shao, D. Yao, H. Gao, Y. Liu, W. Yu, H. Zhang, B. Yang, *ACS Nano* **2017**, *11*, 2239; b) M. K. Gangishetty, S. N. Sanders, D. N. Congreve, *ACS Photonics* **2019**, *6*, 1111; c) J. S. Yao, J. Ge, K. H. Wang, G. Zhang, B. S. Zhu, C. Chen, Q. Zhang, Y. Luo, S. H. Yu, H. B. Yao, *J. Am. Chem. Soc.* **2019**, *141*, 2069.

[22] a) J. F. Liao, Y. F. Xu, X. D. Wang, H. Y. Chen, D. B. Kuang, *ACS Appl. Mater. Interfaces* **2018**, *10*, 42301; b) W. Lv, L. Li, M. Xu, J. Hong, X. Tang, L. Xu, Y. Wu, R. Zhu, R. Chen, W. Huang, *Adv. Mater.* **2019**, *31*, e1900682; c) X. Chen, D. Li, G. Pan, D. Zhou, W. Xu, J. Zhu, H. Wang, C. Chen, H. Song, *Nanoscale* **2018**, *10*, 10505; d) H. Liu, Y. Tan, M. Cao, H. Hu, L. Wu, X. Yu, L. Wang, B. Sun, Q. Zhang, *ACS Nano* **2019**, *13*, 5366; e) A. Loiudice, S. Saris, E. Oveisi, D. T. L. Alexander, R. Buonsanti, *Angew. Chem., Int. Ed.* **2017**, *56*, 10696; f) Q. Xiang, B. Zhou, K. Cao, Y. Wen, Y. Li, Z. Wang, C. Jiang, B. Shan, R. Chen, *Chem. Mater.* **2018**, *30*, 8486; g) V. Malgras, S. Tominaka, J. W. Ryan, J. Henzie, T. Takei, K. Ohara, Y. Yamauchi, *J. Am. Chem. Soc.* **2016**, *138*, 13874.

[23] A. Fakharuddin, F. Di Giacomo, A. L. Palma, F. Matteocci, I. Ahmed, S. Razza, A. D'Epifanio, S. Licoccia, J. Ismail, A. Di Carlo, *ACS Nano* **2015**, *9*, 8420.

[24] C. Sun, Y. Zhang, C. Ruan, C. Yin, X. Wang, Y. Wang, W. W. Yu, *Adv. Mater.* **2016**, *28*, 10088.

[25] Z. Li, L. Kong, S. Huang, L. Li, *Angew. Chem., Int. Ed.* **2017**, *56*, 8134.

[26] a) S. Zhang, W. Lee, *J. Eur. Ceram. Soc.* **2003**, *23*, 1215; b) A. Kawashima, Y. Wang, E. Akiyama, H. Habazaki, K. Asami, K. Hashimoto, *Zairyo to Kankyo* **1994**, *43*, 654.

[27] S. Thapa, K. Bhardwaj, S. Basel, S. Pradhan, C. J. Eling, A. M. Adawi, J.-S. G. Bouillard, G. J. Stasiuk, P. Reiss, A. Pariyar, *Nanoscale Adv.* **2019**, *1*, 3388.

[28] a) F. Zhang, H. Zhong, C. Chen, X.-g. Wu, X. Hu, H. Huang, J. Han, B. Zou, Y. Dong, *ACS Nano* **2015**, *9*, 4533; b) J. Zhou, F. Huang, H. Lin, Z. Lin, J. Xu, Y. Wang, *J. Mater. Chem. C* **2016**, *4*, 7601.

[29] N. Ding, D. Zhou, X. Sun, W. Xu, H. Xu, G. Pan, D. Li, S. Zhang, B. Dong, H. Song, *Nanotechnology* **2018**, *29*, 345703.

[30] B. T. Diroll, G. Nedelcu, M. V. Kovalenko, R. D. Schaller, *Adv. Funct. Mater.* **2017**, *27*, 1606750.

[31] a) S. Huang, Z. Li, B. Wang, N. Zhu, C. Zhang, L. Kong, Q. Zhang, A. Shan, L. Li, *ACS Appl. Mater. Interfaces* **2017**, *9*, 7249; b) C. Carrillo-Carrión, S. Cárdenas, B. M. Simonet, M. Valcárcel, *Chem. Commun.* **2009**, 5214.

[32] Z. Shi, S. Li, Y. Li, H. Ji, X. Li, D. Wu, T. Xu, Y. Chen, Y. Tian, Y. Zhang, *ACS Nano* **2018**, *12*, 1462.

[33] a) Y. Wang, X. Li, S. Sreejith, F. Cao, Z. Wang, M. C. Stuparu, H. Zeng, H. Sun, *Adv. Mater.* **2016**, *28*, 10637; b) S. T. Malak, J. Jung, Y. J. Yoon, M. J. Smith, C. H. Lin, Z. Lin, V. V. Tsukruk, *Adv. Opt. Mater.* **2016**, *4*, 608.

[34] B. Yang, J. Chen, F. Hong, X. Mao, K. Zheng, S. Yang, Y. Li, T. Pullerits, W. Deng, K. Han, *Angew. Chem., Int. Ed.* **2017**, *56*, 12471.

[35] G. E. Eperon, S. N. Habisreutinger, T. Leijtens, B. J. Bruijnaers, J. J. van Franeker, D. W. DeQuilettes, S. Pathak, R. J. Sutton, G. Grancini, D. S. Ginger, *ACS Nano* **2015**, *9*, 9380.

[36] S. Wei, Y. Yang, X. Kang, L. Wang, L. Huang, D. Pan, *Chem. Commun.* **2016**, *52*, 7265.

[37] S. N. Habisreutinger, T. Leijtens, G. E. Eperon, S. D. Stranks, R. J. Nicholas, H. J. Snaith, *Nano Lett.* **2014**, *14*, 5561.

[38] T. Xuan, X. Yang, S. Lou, J. Huang, Y. Liu, J. Yu, H. Li, K.-L. Wong, C. Wang, J. Wang, *Nanoscale* **2017**, *9*, 15286.

[39] H. Liao, S. Guo, S. Cao, L. Wang, F. Gao, Z. Yang, J. Zheng, W. Yang, *Adv. Opt. Mater.* **2018**, *6*, 1800346.

[40] Y. Wei, H. Xiao, Z. Xie, S. Liang, S. Liang, X. Cai, S. Huang, A. A. Al Kheraif, H. S. Jang, Z. Cheng, J. Lin, *Adv. Opt. Mater.* **2018**, *6*, 1701343.

[41] X. Di, Z. Hu, J. Jiang, M. He, L. Zhou, W. Xiang, X. Liang, *Chem. Commun.* **2017**, *53*, 11068.